PAPER

Check for updates

High-capacity adsorption of fluoxetine using olive-stone derived activated biochar: insights into efficiency and mechanism†

Pratishtha Khurana,[a] Samreen Sran,[b] Ratul Kumar Das,[a] Luz Sanchez-Silva[c] and Satinder Kaur Brar [ID] *[a]

The increasing incidences of mood, anxiety, and panic disorders have made fluoxetine (FLX), known for its safety and therapeutic efficiency, one of the most widely prescribed antidepressants globally. However, due to its resistance to natural photolysis and hydrolysis, coupled with the potential to cause endocrine disruption, FLX has become an emerging contaminant, requiring urgent attention for removal. In this context, the present study explores the specific application and integration of physically activated biochar derived from olive stone-an agro-industrial waste-for the targeted removal of FLX. By optimizing activation parameters (CO_2-1000-30-600-1), this study demonstrates the ability to achieve superior adsorption capacities for FLX, which surpass the adsorption capacity of previously reported waste-derived biochar used for FLX removal. The maximum adsorption capacity for the biochar ranged from 4.82 ± 0.04 to 146.45 ± 10.55 mg g^{-1} for initial FLX concentrations of 1 to 50 mg L^{-1}, respectively, for a biochar dose of 0.2 g L^{-1}. Furthermore, the adsorption kinetics data revealed that the biochar–FLX interaction followed the Langmuir adsorption isotherm and a pseudo-second-order kinetic model, indicating irreversible adsorption of FLX onto the homogenous surface of the biochar. Non-electrostatic and non-hydrophobic interactions, such as hydrogen bonding, pore filling, and π–π EDA forces, were identified as the primary interactions facilitating FLX adsorption onto the biochar. This study, therefore, presents a novel approach addressing the dual objectives of environmental remediation and zero-waste principles, contributing significantly to advancing sustainable solutions for emerging contaminants.

1. Introduction

The alarming rates of incidences of psychiatric and mental disorders have led to an increase in the prescription rates and consumption of antidepressants globally. According to a recent report, the defined daily doses (DDD) of anti-depressants per 1000 inhabitants has seen an increase from 13.20 in 2008 to 19.76 in 2018 globally.[1] Fluoxetine (FLX), an anti-depressant from the class of selective serotonin reuptake inhibitors, is the most commonly prescribed anti-depressant globally for the treatment of depression, because of its tolerance, effectiveness, safety and prolonged half-life.[2,3] In the US in 2017, approximately 21 million prescriptions of FLX were filled, suggesting a relatively high level of consumption.[4] However, due to its incomplete metabolism in humans by cytochrome P450

enzymes, whereby 2.5% of the administered dose is excreted unaltered *via* urine, it gets discharged into wastewater.[5]

Due to its resistance to degradation and hydrolysis, and subsequent incomplete removal by WWTPs, has led to its frequent detection in waterbodies across the globe in concentrations ranging between 0.012 to 1.4 mg L^{-1}, causing defects in the behavioral, developmental and reproductive patterns of many aquatic organisms.[6–8] Despite its low concentration, FLX poses a risk to all biomes owing to its ability to cross blood–brain-barrier (BBB) and human placenta due to its lipophilic nature.[9] The drug's uptake in fish has been reported to have consequences on growth and behavior, reproductive axis, metabolism, accumulation, and gene expression.[6,10–14]

With a log K_d = 2.76–3.78 (log K_d > 2.7) and log K_{ow} > 4, adsorption appears as a robust, effective, and efficient tertiary method to enhance its removal and limit its exposure in environment.[15–17] Furthermore, with increasing emphasis on principles such as zero waste and circular economy, the production of waste-derived bio-adsorbents and their application in remediating FLX-polluted waters have been extensively researched.[18–20] However, their low adsorption capacities have proven insufficient. For instance, biosorbents derived from agri-food waste have shown a maximum adsorption capacity of

[a]*Department of Civil Engineering, Lassonde School of Engineering, York University, Ontario, Canada. E-mail: satinder.brar@lassonde.yorku.ca*

[b]*Department of Biology, York University, Ontario, Canada*

[c]*Department of Chemical Engineering, University of Castilla-La Mancha, Spain*

6.41 mg g^{-1}, as reported for biochar obtained from eucalyptus when tested with FLX$_0$ of 20 mg L^{-1}.[18] A similar study by Silva *et al.*, (2020) investigated the maximum adsorption capacities of waste-based biosorbents derived from cork waste, spent coffee grounds, and pine bark for FLX$_0$ 5 mg L^{-1}, which ranged between 4.74–14.31 mg g^{-1}.[20] In this regard, the present study explores the application of physically activated biochar derived from olive stone for the removal of FLX. While the valorization of olive oil production residues, such as olive stones, has been explored to some extent, their specific application in biochar production and other sustainable materials remains an emerging area of research.[21] The novelty of this study lies in the use of these residues combined with physical activation (using CO_2 and steam) to create biochar for environmental remediation. This innovative approach not only highlights the potential of olive oil production residues but also introduces a sustainable alternative to chemical activation methods. The physical activation method, using CO_2 and steam, offers several advantages over chemical activation. It is more sustainable and environmentally friendly, as it does not require aggressive chemicals, thus reducing toxic byproducts and minimizing environmental impact. Additionally, it produces fewer hazardous waste materials, making it more compatible with circular economy principles.[21,22] The process also allows for precise control over biochar properties, such as surface area and porosity, which is crucial for its application in environmental remediation. Furthermore, physical activation can be more adaptable to various types of biomasses, more energy-efficient in certain cases, and better suited to comply with stringent environmental regulations, making it a versatile and cost-effective approach.[21] The novelty of this activation method, alongside its environmental benefits, further strengthens the innovative nature of this study.

The present study, thereby, demonstrates specific application and integration of physically activated biochar derived from olive stone, an agro-industrial waste, for the targeted removal of FLX. This emerging pharmaceutical contaminant presents unique environmental challenges due to its resistance to natural degradation and its endocrine-disrupting potential, making its remediation an underexplored yet critical area of research.

2. Experimental

2.1 Materials and methods

Fluoxetine hydrochloride (FLX, >98%) was purchased from Sigma Aldrich (Toronto, Canada). An appropriate amount of the salt was dissolved in water to prepare the stock solution of FLX, which was stored in a dark glass vial at 4 °C until use. The olive stone waste was kindly received from an oil mill in Toledo, Spain (Aceites Garcia de la Cruz). It is worth mentioning that the olive stone was milled to obtain a particle size of 2–4 mm for pyrolysis and activation without any drying.

2.2 Biochar preparation and activation methods

Biochar was prepared by a single-step physical activation process, using olive stone as a low-carbon precursor and steam or carbon dioxide as the activation agents in a bench-scale high-pressure thermobalance (Linsesis STA HP/2 HP-TGA DSC). The biomass was carbonized by heating it to 600 °C at a heating rate of 10 °C min^{-1}, and resting for 60 minutes, under N$_2$ (300 N mL min^{-1}). The carbonized material was then subjected to physical activation using steam or CO_2 under different operating conditions for temperature (700–1000 °C) at a heating rate of 20 °C min^{-1} under N$_2$ atmosphere, pressure, holing time (30–60 min), and flow rate (CO_2: 300–600 N mL min^{-1}; steam: 0.07–0.3 N mL min^{-1}), as summarized in Table S1.†

Before use, the biochar samples were lightly crushed using a stainless-steel mortar pestle set and passed through metal sieves to obtain a fine powder (25–63 μm) and stored at room temperature until use.

2.3 Biochar characterization

The prepared biochar samples were characterized for their surface area and porosity (Brunauer–Emmett–Teller (BET)), elemental content (CHNS analyzer), zeta potential, and cation exchange capacity (CEC). The selected biochar (biochar 7, CO_2-1000-30-600-1) was also characterized by FTIR for surface functional groups, point of zero charge (pHzc) to understand the conformational changes with varying pH. Morphological features of the biochar were observed *via* imaging with Scanning Electron Microscope (SEM). The sample preparation methods for all the techniques are outlined in the Text 1 of the ESI.†

2.4 Preliminary adsorption assays for biochar screening

For screening the biochar, preliminary adsorption experiments were performed with 5 mg of respective biochar in 10 mL of FLX solution (0.5 to 50 mg L^{-1}) at room temperature. The initial FLX concentration was deliberately maintained high to (i) ensure accurate quantification of the drug and (ii) sought the saturation limit of the biochar. The samples were equilibrated for 24 hours on an end-to-end shaker, followed by centrifugation (Sorvall ST 16, Thermo Fisher Scientific, USA). The resulting supernatant was then analyzed for FLX using LC-MS (Text 3 in ESI†). The samples were analyzed in duplicates and the removal percentage was calculated as:

$$\text{Removal}(\%) = \frac{C_0 - C_t}{C_0} \times 100 \tag{1}$$

where C_0 and C_t represent FLX concentrations (mg L^{-1}) at time 0 (initial) and t (24 h, here). Based on the preliminary screening, one biochar activated with steam, and one activated with CO_2 were selected for further evaluation using secondary screening method.

For the successive screening, the selected steam- and CO_2-activated biochar (10 mg/50 mL) was used to perform FLX removal kinetics with an initial concentration of 50 mg L^{-1}. The percentage of FLX removal was determined using eqn (1). The biochar with faster kinetics was selected for the rest of the study.

2.5 Adsorption and kinetic studies

Adsorption studies were performed by adding the selected biochar to 50 mL FLX aqueous solution at room temperature

with continuous stirring at 400 rpm for 2 hours. The effect of (i) initial dose of FLX (1, 5, 10, 25, and 50 mg L^{-1}); (ii) time (0, 5, 10, 20, 40, 60, and 120 minutes); and (iii) dose of biochar (10 and 20 mg for FLX 25 and 50 mg L^{-1}) were investigated. Commercial activated bamboo charcoal powder was used as a reference. The samples were regularly collected and analyzed for residual FLX using UV-visible spectroscopy (λ_{max} 226 nm) and LC-MS for lower concentrations (<5 mg L^{-1}) after centrifugation to remove the adsorbent.

The adsorption capacity (q_t (mg g^{-1})) was calculated using the eqn (2):

$$q_t = (C_0 - C_t) \times \frac{V}{m} \qquad (2)$$

where m (g) is the mass of the biochar used, and V (L) is the volume of the solution.

Subsequently, to understand the kinetics and the behaviour of adsorption, the experimental data was fit to different adsorption isotherm models (Langmuir and Freundlich) and kinetic models (pseudo-first order (PFO), pseudo-second order (PSO), and intra-particle diffusion (IP)), as described in Text 2 in the ESI.†

2.6 Regeneration and reusability

In order to investigate the regeneration and reusability of the spent biochar, solvent desorption assays were performed by changing solvent strength. For this, the residues from equilibrium adsorption experiments (25 mg L^{-1} FLX) were recovered by centrifugation and overnight drying at 45 °C. To evaluate the desorption, the 2 mg of spent biosorbent was then mixed with 5 mL of different extraction solvents (i) water, (ii) MeOH, (iii) MeOH (pH adjusted to 2 using 0.1 M HCl), and (iv) 50% ACN in water, under end-to-end shaking for 24 hours at room temperature. This was followed by centrifugation and determination of desorbed FLX in the supernatant using UV-visible spectroscopy and LC-MS method. The desorption efficiency was calculated using eqn (3.)

$$\text{Desorption effeciency} = \frac{C \times V}{q \times m} \times 100\% \qquad (3)$$

where C (mg L^{-1}) is the desorbed FLX concentration. The biochar was then regenerated by lyophilization.

In addition to solvent desorption, an advanced regeneration method combining Fenton's oxidation with ultra-sonication (Ferro-sonication; Fe-UlS), as mentioned elsewhere, was also investigated.[23] For this, the spent biochar was suspended in 10 mL Milli-Q, to which 1 : 1 %v/v Fenton's reagent (0.05 M FeSO$_4$ and H$_2$O$_2$) was added, and acidic pH (2.5) was adjusted using H$_2$SO$_4$. The solution was then sonicated at 40 kHz for 30 minutes, followed by centrifugation, washing with water, and lyophilization to obtain the regenerated biochar. The regenerated biochar (both solvent and Fe-UlS) was analysed for residual FLX by using Thermogravimetric Analyser (TGA) (Discovery TGA55, TA instruments, USA) at a heating rate of 10 °C min^{-1} for a temperature range of RT (~20 °C) to 500 °C.

2.7 Adsorption mechanism

To determine the adsorption mechanism and investigate the contribution of electrostatic and hydrophobic interactions in facilitating the adsorption of FLX on the surface of biochar, the effect of pH (3–11), NaCl (0.01, 0.1, and 0.5 M) and MeOH (2.5, 5, and 10% v/v) on the adsorption capacity of biochar was investigated for [FLX]$_0$ 25 mg L^{-1}. The samples were collected at regular intervals (0, 5, 10, 20, 40, 60, and 120 minutes) and analyzed for residual FLX using UV-visible spectroscopy (λ_{max} 226 nm). ANOVA was used to determine their statistical significance with a p-value of 0.05 as the level of significance.

3. Results and discussion

3.1 Biochar characterization and screening

BET technique, CHNS analysis, and CEC, as summarized in Table S2,† were used to characterize the biochar samples for their surface area and pore size distribution. The results indicated that the biochar 3 (H$_2$O-900-30-0.15-1) had the largest surface area (1015 m^2 g^{-1}) followed by biochar 4 (836 m^2 g^{-1}, H$_2$O-900-30-0.07-1)–biochar 2 (828 m^2 g^{-1}, H$_2$O-800-60-0.3-1), and biochar 5 (678 m^2 g^{-1}, H$_2$O-800-60-0.15-1). Biochar 1 (449 m^2 g^{-1}, H$_2$O-700-60-0.3-1) had the lowest surface area, as recorded by the surface area analysis. It is evident, both-here and from previous reports, that the surface area increases with the increasing activation temperature because of the removal of carbon atoms from the surface.[22] This can also be rationalized with the carbon content of steam-activated biochar, which follows the order biochar 3 (%C 69.6, 900 °C)> biochar 4 (%C 73.5, 900 °C)> biochar 2 (%C 76.1, 800 °C)–biochar 5 (%C 874.5, 800 °C)> biochar1 (%C 83.5, 700 °C). Overall, the total carbon content in all biochar samples ranged from 63.3% to 83.5%, $i.e.$, medium carbon content, as previously described by Lehmann et $al.$[24] Correspondingly, the % oxygen for all the biochar samples varied from 13.94% to 32.83%.

Similarly, for CO$_2$ activation, the biochar followed the order: biochar 7 (855 m^2 g^{-1}) > biochar 8 (775 m^2 g^{-1}) >biochar 10 (557 m^2 g^{-1}) >biochar 9 (382 m^2 g^{-1}) > biochar 6 (236 m^2 g^{-1}) for surface area. In general, surface area increases with rising activation temperature from and improving flow rate from 300 to 600 mL min^{-1} and decreases with time, as seen in Table S2.† Additionally, the zeta potential of physically activated biochar (1–10) was close to 0 mV (data not shown), which indicates the presence of both positive and negative charges, and rapid coagulation or aggregation of the particles in the solution.

Adsorption experiments were performed to screen for the selected biochar. Batch adsorption assays were performed at room temperature for 24 hours, and the results are shown in Fig. S1.† As seen in Fig. S1a,† steam-activated biochar removed a significant portion of the drug, except biochar 1, where the activity drastically reduced when the FLX concentration gradually increased from 0.5 to 50 mg L^{-1}. Biochar 4 performed unfailingly throughout the drug concentration and was selected for the rest of the study. Similarly for the CO$_2$-activated biochar set, as the concentration of FLX increased from 0.5 to 50 mg L^{-1}, a significant reduction in % adsorption of FLX was

seen for biochar 6 (from 94.99 ± 4.59 to 22.64 ± 0.09) and 9 (from 96.37 ± 3.46 to 31.55 ± 0.67), while gradual decrease was seen in the reactivity of biochar 8 and 10, where % removal of FLX decreased from 99.87 ± 3.48 and 99.81 ± 0.10 to 76.81 ± 4.97 and 76.48 ± 23.01, respectively (Fig. S1b†). For biochar 7, only a slight change in activity was seen (from $99.25 \pm 0.73\%$ to $92.20 \pm 3.92\%$) and thus selected for the rest of the experiments.

Therefore, based on the results of the batch adsorption studies, steam-activated biochar 4 and CO_2-activated biochar 7 were selected for the next set of the experiments. To select one of the two biochar, the adsorption kinetics for removal of FLX was performed with 50 mL 50 mg L^{-1} FLX with 10 mg biochar 4 and biochar 7. As shown in Fig. S1† CO_2-activated biochar 7 demonstrated a faster removal than steam-activated biochar 4, with residual FLX concentrations of 7.142 ± 2.48 mg L^{-1} and 16.515 ± 1.67 mg L^{-1}, respectively, after 1 h of contact. Thereby, biochar 7 was selected for the rest of the study. The pHzc of the selected biochar 7 was observed to be about 7, as shown in Fig. S1b.† Also, the obtained FTIR spectra (Fig. S1c†) for the biochar indicated the presence of O-rich functional groups including carbonyl, carboxylic, and alcohols (Table S3†).[18]

The SEM analyses of the untreated, pristine biochar 7 (CO_2-1000-30-600-1) revealed a rough texture, heterogeneous surface, irregular granular morphology, and highly porous matrix with interconnected pores (Fig. 1A(i); magnification 200×). The grain size and high porosity could be attributed to the high pyrolysis temperature and CO_2-activation. When pyrolyzed at 1000 °C,

the carbon tends to become crystalline and larger in grain size, as observed previously.[25] The magnified image (5000×, Fig. 1B(I)) displays the porous structure network of interconnected micropores with variable pore size distribution. Furthermore, the pore size distribution of the selected biochar 7, as determined using BET, predominantly indicates the presence of only micropores (<2 nm) (Fig. S2†).

3.2 Adsorption kinetics

The kinetic assays of FLX (1, 5, 10, 25, and 50 mg L^{-1}) with olive-stone derived CO_2-activated biochar 7, as shown in Fig. 2a, indicate that FLX removal occurs rapidly in the first 5 minutes of contact. For lower initial concentrations of FLX (1 and 5 mg L^{-1}), equilibrium was attained within 5 minutes with 100% removal of FLX. For 10 mg L^{-1} FLX, equilibrium and 100% removal were achieved within 10 minutes of the assay. Further, as can be seen in Fig. 2a, for higher concentrations (25 and 50 mg L^{-1} FLX), the minimum time required to attain equilibrium was <20 minutes, as reported previously.[18,25,26] The performed kinetic studies show that after 2 h of exposure, the amount of FLX adsorbed on the surface of biochar ranged from 4.82 ± 0.04 mg g^{-1} to 146.45 ± 10.55 mg g^{-1}, for initial FLX concentrations of 1 mg L^{-1} to 50 mg L^{-1}, respectively (Fig. 2b). While commercial bamboo activated charcoal, which was used as a reference, exhibited maximum adsorption capacity of 9.85 ± 4.83 mg g^{-1} and a removal efficiency of $4.09 \pm 2.07\%$ after 2 h of contact with 50 mg L^{-1} FLX (Fig. 2a and b). The uptake of FLX can also be traced by EDS mapping of F, as shown in Fig. 1C(iii).
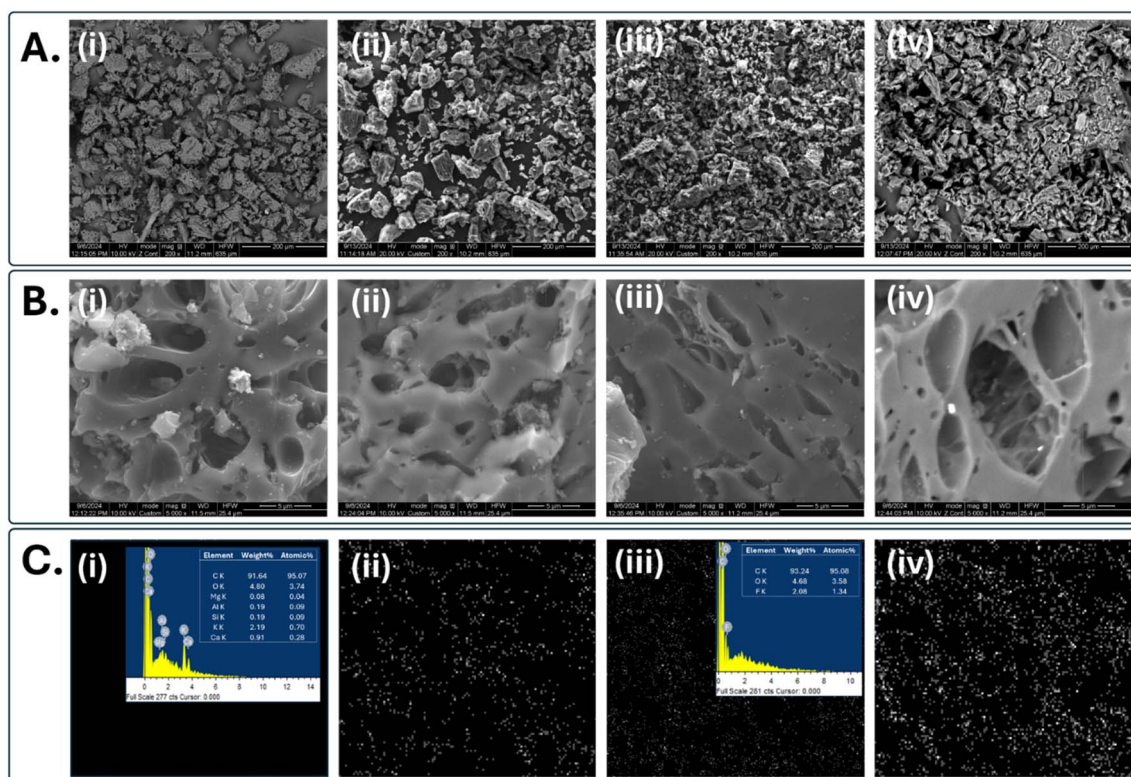

Fig. 1 SEM images of (i) Untreated biochar, (ii) Biochar loaded with 1 mg L^{-1} FLX, (iii) Biochar loaded with 25 mg L^{-1} FLX, and (iv) biochar after desorption with MeOH for at magnification (A) 500×, (B) 5000× (C) Shows EDS mapping for fluorine atom, inset shows EDS spectrum.
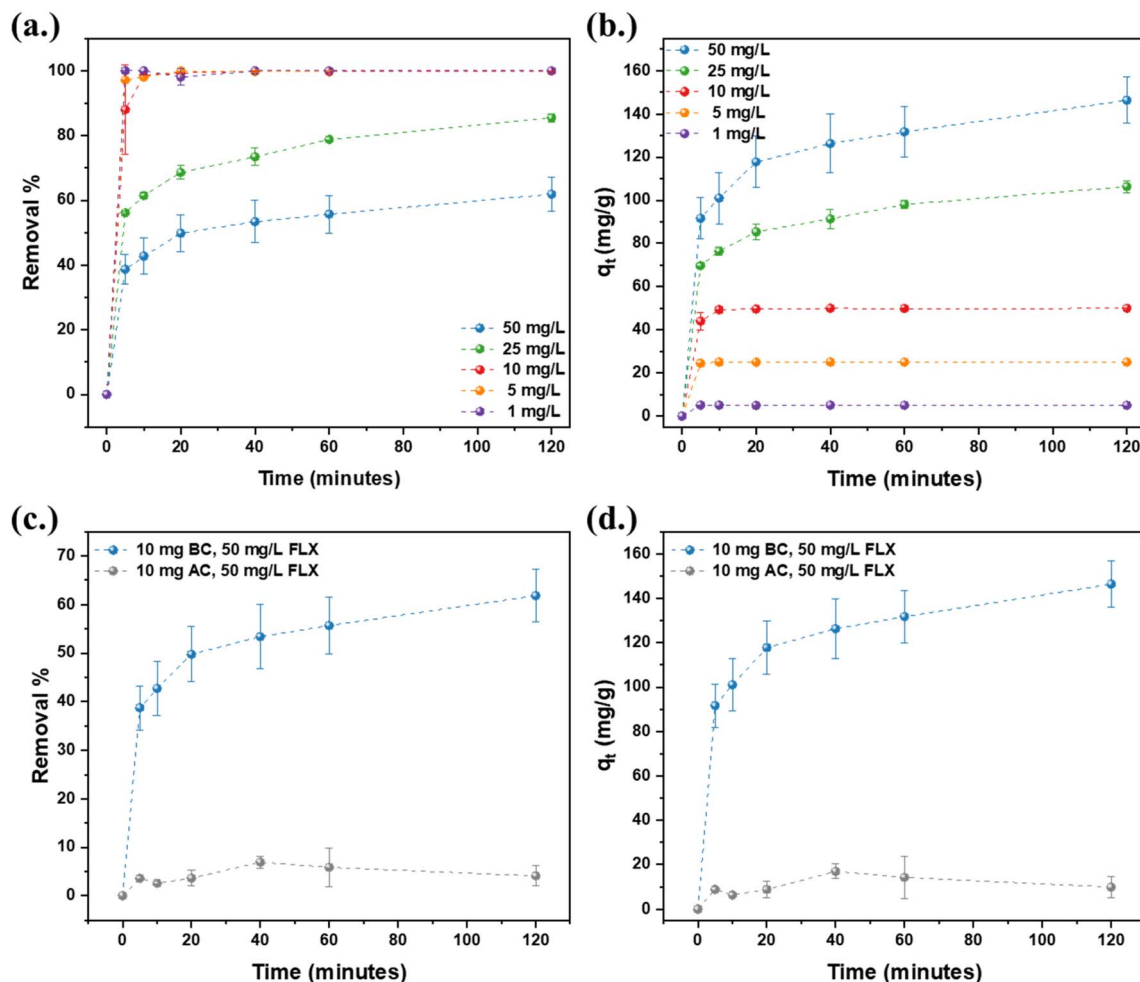
Fig. 2 (a) Removal efficiency, and (b) uptake (q_t) of FLX by biochar 7 for FLX concentrations of 1, 5, 10, 25, and 50 mg L^{-1} for 0–120 minutes; (c) removal efficiency, and (d) uptake (q_t) of FLX by biochar 7 and commercially available activated charcoal for FLX concentration of 50 mg L^{-1} for 0–120 minutes.

For the biochar saturated with 25 mg L^{-1}, EDS mapping shows 2.08 wt% or 1.34 atomic% in the mapped area. However, no morphological changes were observed for the biochar.

The uptake potential of the prepared olive-stone biochar (146.45 ± 10.55 mg g^{-1} within 2 h for $[C_0] = 50$ mg L^{-1} FLX) surpasses the adsorption capacity of previously reported waste-derived biochar used for FLX removal. Some of these recent studies are summarised in Table 1 for comparison. For instance, a study by Fernandes (2019) reported the attainment of equilibrium of agri-food waste derived biosorbents after 15 minutes of the assay, with a maximum adsorption capacity of 6.41 mg g^{-1} for biochar obtained from eucalyptus for FLX_0 20 mg L^{-1}, while olive-stone biochar achieved a q_{max} of 106.32 ± 2.73 mg g^{-1} (>16 fold increase).[18] Similarly, a recent study by Escudero-Curiel et al., (2023) utilised nitrogen-doped alperujo derived hydrochars to remove FLX with q_{max} of 111.63 mg g^{-1} urea-modified hydrochar, while polyethyleneimine-modified adsorbent achieved a q_{max} of 29.31 mg g^{-1} for FLX.[27] Silva et al., (2020) investigated the maximum adsorption capacities of waste-based biosorbents derived from cork waste, spent coffee

grounds, and pine bark for FLX_0 5 mg L^{-1}, which ranged between 4.74–14.31 mg g^{-1};[20] whereas, the present study achieves a q_{max} of 25 mg g^{-1} for FLX_0 5 mg L^{-1}. In addition to agri-food waste, xylan, pectin, and lignin were also explored for their potential to removal FLX from aqueous solutions. For instance, Farghal et al., (2023) studied the ability of xylan and pectin coated activated-carbon (XCM and PCM) based magnetite adsorbents to adsorb FLX and achieved a maximum adsorption capacity of 90.9 mg g^{-1} and 114.9 mg g^{-1}, respectively.[28] A similar study with lignin-derived anionic nanofibers demonstrated a capacity of 29 mg g^{-1}.[29] It is worth mentioning that the olive-stone derived CO_2-activated biochar performed better for FLX removal than some of the previously reported commercial adsorbents. For example, commercial carbon aerogel (NANOLIT 3D monolith NQ40 honeycomb premium) (CO_2 activated), with a specific surface area of 790 m^2 g^{-1}, obtained an adsorption capacity of 125.24 mg g^{-1} at pH 7–7.5.[30] Similarly, an adsorption capacity of 96.2 mg g^{-1} was observed for commercial activated carbon PBFG4 in a study by.[31] Therefore, CO_2-activated biochar (CO_2-1000-30-600-1) used in the present study demonstrates the

Table 1 Comparison of maximum adsorption capacities of FLX by different waste-derived adsorbents

Waste-derived biosorbent	q_{max} (mg g^{-1})	pH	Initial concentration (mg L^{-1})	Temperature (°C)	References
Eucalyptus biochar	6.41	6.5	20	RT	Fernandes et al., 2019 [18]
Alperujo biochar	4.63, 5.95	6.4	30	RT	Escudero-Curiel et al., 2023 [27]
Nitrogen – doped alperujo Biochar	16.09, 111.63	6.4	30	RT	Escudero-Curiel et al., 2023 [27]
Fish bone char	55.87	—	100	—	Piccirillo et al., 2017 [25]
Spent coffee ground	14.31	9	5	RT	Silva et al., 2020 [20]
Pine bark	6.53	9	5	RT	Silva et al., 2020 [20]
Cork waste	4.74	9	5	RT	Silva et al., 2020 [20]
Nanofiber AL : PVA 50 : 50	29	—	50	—	Camiré et al., 2020 [29]
Nanocomposite XCM	90.9	7.35	25	28	Farghal et al., 2023 [28]
Nanocomposite PCM	114.9	7.35	25	28	Farghal et al., 2023 [28]
Pine-bark biosorbents	0.652	—	5	25	Lago et al., 2024 [19]
Olive-stone biochar	4.82–146.45	6–7	1–50	RT	This study

ability to achieve superior adsorption capacities for FLX. Further, FLX removal combined with the valorization of agricultural residues, represents a novel approach that addresses the dual objectives of environmental remediation and zero-waste principles. We believe this integration fills an important research gap and contributes to advancing sustainable solutions for emerging contaminants.

A higher adsorbent dose of 20 mg/50 mL was also studied for initial FLX concentrations of 25 and 50 mg L^{-1}, as shown in Fig. 3. For initial FLX concentration 25 mg L^{-1}, biochar dose of 10 mg removed $85.49 \pm 1.22\%$ FLX with maximum uptake capacity of 106.32 ± 2.73 mg g^{-1}, while adsorbent dose 20 mg could remove $99.10 \pm 0.18\%$ of FLX with adsorption capacity of 125.27 ± 0.90 mg g^{-1} (Fig. 3a and b). Similarly, for 50 mg L^{-1} FLX, 10 mg of olive-stone derived biochar had a removal efficiency of 61.87 ± 5.39 and an uptake of 146.45 ± 10.55 mg g^{-1}, while 20 mg of biochar removed $93.35 \pm 3.62\%$ FLX with q_t of 230.56 ± 15.48 mg g^{-1} (Fig. 3c and d). This is markedly better than other reported agri-food waste derived adsorbents and comparable to the maximum adsorption capacities of commercial adsorbents explored by Silva et al., (2020), which ranged between 21.86–233.50 mg g^{-1}.[20]

To further understand the kinetics of the adsorption, the experimental data was fit into the PFO, PSO, and IP models (Fig. S3†). The model parameters as obtained are shown in Table 2. A comparative analysis of the model parameters reveals that the correlation coefficient of the PSO rate equation is higher than that of the PFO kinetics equation, thereby suggesting that the adsorption of FLX onto biochar follows PSO kinetics. Since high-fitting correlations to PFO and PSO have often been related to physisorption and chemisorption, respectively; the adsorption of FLX in the present study indicates chemisorption. However, physicochemical properties of both adsorbate and adsorbent, activation energy, and thermodynamic parameters, as mentioned elsewhere, play a crucial role in the adsorption mechanism.[32]

Also, it is noteworthy that both the kinetic models- PSO and PFO, exclude mass transfer considerations. Since the olive-stone-derived biochar is highly porous with internal pores accessible to FLX and the media, consideration of mass

transfer, and external and internal diffusion becomes important. Thereby, to determine diffusion and rate limiting step during adsorption, the experimental data was fit to IP diffusion model.

The model parameters- C (mg g^{-1}) and rate constant (K_p), as determined from the intercept and slope of the linear plot of q_t vs. $\sqrt{t}$ (Fig. S3c†), respectively, are shown in Table 2. Since the plot does not pass through origin, the intraparticle diffusion model plot, demonstrates that there are more than one rate-limiting steps for the adsorption of FLX onto the surface of biochar. The plot can be divided into two zones-zone I, and zone II, with different slopes. In zone I, the slope is steeper, indicating the adsorption of FLX molecules onto the macropores of the biochar and the existence of diffusion film.[30] While zone II is associated with the diffusion of FLX into the microporous structure of biochar. Further, the greater the value of the y-intercept, the more is the intraparticle diffusion.[30,33] Since the y-intercept (i.e., C (mg g^{-1})) is greater in zone II compared to zone I, the process is driven by intra-particle diffusion.

For lower initial FLX concentrations of (1 and 5 mg L^{-1}), the plateau in both zone I and zone II indicate that the system has reached equilibrium. For a concentration of 10 mg L^{-1}, zone I suggests the simultaneous occurrence of both film and intra-particle diffusion, while zone II represents equilibrium. Similarly, for higher concentrations (25 and 50 mg L^{-1}), both zone I and zone II indicate a concurrent occurrence of film and intra-particle diffusion, as mentioned previously.[30,34] As the initial concentration of FLX increases from 1 to 50 mg L^{-1}, the value for the boundary thickness (C) also increases. Larger the intercept, more the boundary layer effect. Also, as shown in Table 2, the value of K_p also increases with increasing initial concentration of FLX, indicating a direct correlation between FLX concentration and the intra-particle diffusion.[35,36]

3.3 Adsorption isotherm

To understand the adsorption behavior and predict the nature of adsorption mechanisms, the experimental data was fit into the Langmuir and Freundlich isotherm models (Fig. S4†). The fitting coefficients and statistical parameters for both models are summarised in Table 3. These parameters show that both
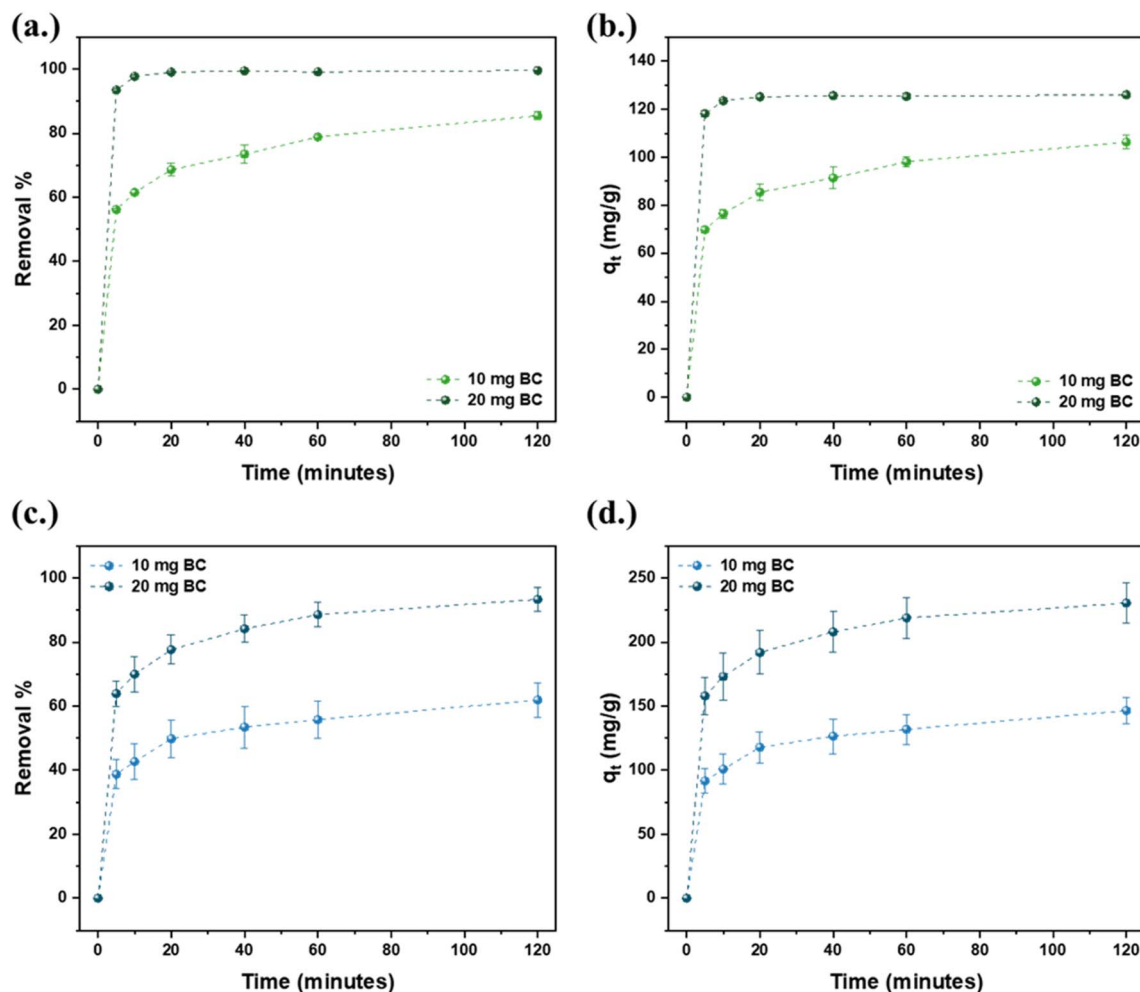
Fig. 3 (a) Removal efficiency, and (b) uptake (q_t) of FLX by biochar 7 for FLX concentrations of 25 mg L^{-1} for 0–120 minutes; (c) removal efficiency, and (d) uptake (q_t) of FLX by biochar 7 for FLX concentration of 50 mg L^{-1} for 0–120 minutes.

Table 2 Rate constants (k_1, k_2, and K_p) obtained for different initial concentrations of FLX by PFO, PSO, and intraparticle diffusion kinetic model

FLX (mg L^{-1})	PFO			PSO			IP (zone I)			IP (zone II)		
	q_e (mg g^{-1})	k_1 (min^{-1})	R^2	q_e (mg g^{-1})	k_2 (g mg^{-1} min^{-1})	R^2	C (mg g^{-1})	k_p (mg g^{-1} min^{-1})	R^2	C (mg g^{-1})	k_p (mg g^{-1} min^{-1})	R^2
50	65.366	0.031	0.662	141.844	0.002	0.994	65.092	11.686	0.992	98.059	4.408	0.997
25	75.944	0.050	0.648	102.459	0.004	0.994	54.065	7.031	0.999	75.232	2.869	0.940
10	49.402	0.168	0.785	49.652	0.061	1.000	38.102	2.301	0.997	49.057	0.037	0.999
5	24.532	0.130	0.584	24.704	2.128	1.000	24.603	0.009	0.990	24.287	0.065	1.000
1	4.759	0.121	0.516	4.751	1.064	1.000	4.268	0.099	0.879	4.757	−0.004	0.757

the isotherm model fit the experimental data with good regression coefficients. From a comparative analysis of model parameters, it is evident that Langmuir isotherm model was the better fit for the obtained data, with higher values for linear regression coefficients ($R^2 > 0.98$). As the experimental data aligns best with Langmuir isotherm, the separation factor, R_L, can be appropriately determined using eqn (4).[35,37]

$$R_L = \frac{1}{1 + bC_0} \quad (4)$$

where C_0 is the initial concentration of FLX. It is a dimensionless equilibrium parameter to understand the feasibility of the adsorption behavior of FLX onto the adsorbent. Based on the value of R_L, the process of adsorption can be unfavorable ($R_L > 1$), linear ($R_L = 1$), favorable ($0 < R_L < 1$) and irreversible ($R_L = 0$).[32,35] For the experimental data, the value of R_L varied between 0.324 and 0.986, i.e., $0 < R_L < 1$, thereby suggesting favourable adsorption of FLX onto the biochar for initial FLX concentrations varying from 1 to 50 mg L^{-1}.[32,35] Also, as the initial FLX concentrations increased from 1 mg L^{-1} to 50 mg L^{-1}, the

Table 3 Langmuir and Freundlich isotherm model parameters of adsorption of FLX on biochar

FLX (mg L^{-1})	Langmuir isotherm				Freundlich isotherm		
	Q_0 (mg g^{-1})	b (L mg^{-1})	R_L	R^2	K_F [(mg g^{-1}) (L mg^{-1})]$^{1/n}$	$1/n$	R^2
50	58.514	0.003	0.860	0.976	2419.390	0.961	0.975
25	58.140	0.001	0.986	0.991	183.950	0.395	0.959
10	44.723	0.060	0.626	0.997	47.350	0.02	0.735
5	97.371	0.088	0.695	1.000	23.104	0.024	0.967
1	4.382	2.082	0.324	0.999	3.950	0.062	0.940

highest maximum monolayer adsorption (Q_0 (mg g^{-1})) ranged from 4.38 to 58.51 mg g^{-1}, respectively. The observed maximum monolayer adsorption was higher than that obtained for high-surface-area nanoparticles reported previously (40.7 mg g^{-1} for RuFeO$_3$ and 15.8 mg g^{-1} for CeFeO$_3$).[35]

In addition, the model parameters obtained by data fitting to Freundlich isotherm model (as shown in Table 3) further provide insight into the adsorption of FLX onto the surface of the biochar. For instance, the values for K_F >1 indicate strong adsorption capacity, $0 < K_F < 1$ suggests favorable irreversible adsorption, while $K_F = 1$ for linear isotherm. As shown in the Table 3, K_F values of 3.95, 23.10, 47.35, 183.95, and 2419.39 were observed for [FLX]$_0$ 1, 5, 10, 25 and 50 mg L^{-1}, respectively, which represents that favourable irreversible adsorption. That is, olive-stone derived biochar has a high capacity for adsorbing FLX from its aqueous solution. The heterogeneity factor, $1/n$, also suggests favourable adsorption ($0 < 1/n < 1$). Typically, $1/n$ closer to 0 indicates that the adsorption intensity is higher.[18]

3.4 Regeneration and reusability tests

To desorb the adsorbed FLX and regenerate the spent biochar, solvents with different polarities were used as eluents and the results are summarized in Fig. S6a.† Since solvent polarity affects the contaminant desorption, a polar protic solvent (methanol) and a dipolar aprotic solvent (50% ACN) were employed for the study. Deionized water was used to verify desorption at equilibrium. A very low recovery rate of 0.06 ± 0.03% was observed with water, indicating that the bond strength was sufficient to prevent the establishment of a new equilibrium.[32]

Methanol has often been used as a desorption solvent owing to its ability to disrupt polar interactions, such as hydrogen bonding, that may exist between the adsorbate and the surface of the adsorbent. It was also identified as the best desorption solvent for the recovery of FLX from nanofibers, with 100% recovery.[29] However, in the present study, only 21.51 ± 2.44% desorption was observed. Similarly, pH-adjusted MeOH (pH 2), under low magnetic stirring at 30 °C, performed best for the desorption of FLX from the chitosan-derived hydrogel beads, thereby achieving >95% desorption.[32] However, in the present study, this solvent could only desorb 19.83 ± 4.78% after 24 h of stirring at room temperature. This can be explained by the nature of forces acting between FLX and the adsorbent in both studies. The study by Nkana et al., (2024) suggested the physisorption of FLX on active sites of the biosorbent, while in the

present study, the adsorption of FLX on biochar is attributed to chemisorption and intra-particle diffusion.[32]

Acetonitrile is another solvent popularly used as an eluent. In a recent study by Lago et al., (2024), 50% acetonitrile (% v/v) was found to be the best desorption solvent for FLX from pine-bark-derived biosorbents with 100% desorption within 48 h.[19] The present study observed 19.02 ± 3.26% desorption with 50% acetonitrile, indicating a strong interaction, such as pore filling and/or strong π–π stacking, between FLX and the surface of the biochar. This also highlights the need for advanced regeneration methods to recover the porosity of the spent biochar without altering the structural parameters.

Previous studies have suggested the use of solvent-free techniques, such as the Fenton and Fenton-like process with peroxymonosulphate (PMS), to regenerate the spent biochar and subsequent cost reduction.[26,30] However, the use of strong oxidants, such as hydrogen peroxide, can often result in the collapse of pores by introducing oxygen-rich functional groups on the walls and at the entrance of the pores, as observed in the present study.[30,38,39] Despite this loss of porosity, Fe-UlS regenerated biochar retained 38.78 ± 1.59% removal efficiency for cycle 2 of adsorption with 25 mg L^{-1} FLX after 2 h of treatment (as shown in Fig. S6b†). This decrease in FLX uptake can be attributed to the blocking of pores due to oxidation and loss of potential interaction sites of FLX and biochar.[39] Further, a comparative analysis of TGA curves of unused and regenerated biochar shows an additional weight loss between 200–400 °C, thereby suggesting the presence of residual FLX in the biochar regenerated using solvents. While Fe-UlS regenerated biochar shows higher mass loss than raw biochar, but less than solvent-regenerated biochar. This indicates either more effective desorption of FLX by the synergistic action of Fe-catalysed oxidation and ultrasound. However, in practical application, the dose of the oxidant and the treatment time for regeneration can be optimized to maximize the retention of the porous network, without altering the surface of the adsorbent.[39]

3.5 Adsorption mechanism

The exchanges between the adsorbent and the adsorbate, and the subsequent removal by effective adsorption, can occur through one or more of these chemical interactions- (i) electrostatic attractions between functional groups of the adsorbate and the adsorbent owing to their opposing electrical charges, (ii) hydrogen bonding or dipole–dipole interactions, (iii) hydrophobic, (iv) π–π electron-donor-acceptor (EDA) interactions, and (v) pore filling.[19,40]
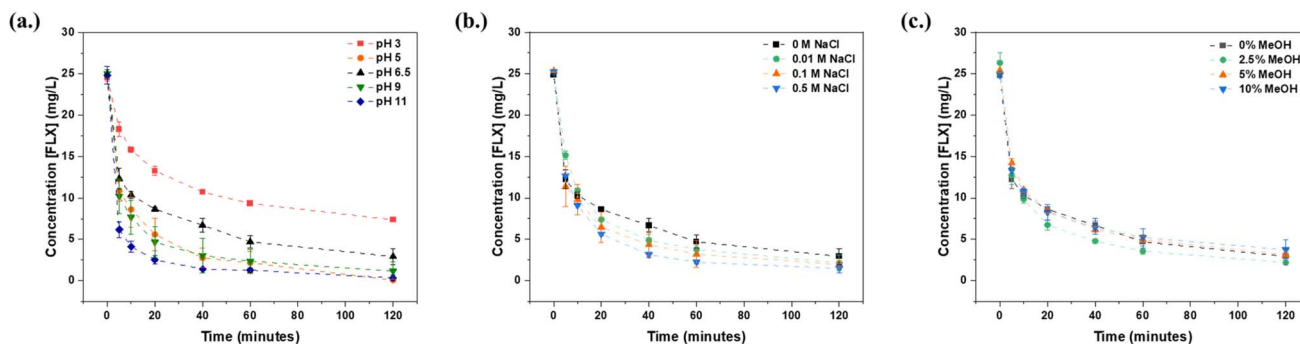
Fig. 4 Effect of (a) pH, (b) NaCl (ionic strength), and (c) MeOH (organic solvent) on the adsorption of FLX (C_0 25 mg L^{-1}) onto biochar.

The adsorption *via* electrostatic interactions is governed by the surface charge of the adsorbent and the adsorbate, ruled by the pHzc and pK_a, respectively. The pHzc of the synthesized biochar was observed to be around 7, *i.e.*, it has positive and negative charges that balance to give electrically neutral biochar. When the pH of the solution is less than pHzc, the surface of the biochar is positively charged, favouring the adsorption of anionic species.[41] Meanwhile, for pH > pHzc, the negative surface charge of the biochar favours the adsorption of cationic species *via* electrostatic attraction. The pK_a of FLX is 9.8, suggesting the presence of FLX as a cationic species at circumneutral pH.[19,20] Therefore, under the conditions of the study (6 < pH < 7), when the biochar is electrically neutral (with slightly more positive charge) and FLX is positively charged, weak electrostatic forces are expected. For the solution pH < 7 (pH = 3 and pH = 5), where both FLX and biochar surface are positively charged, electrostatic repulsion is expected, while at pH = 9 electrostatic attraction is predicted due to the opposite charge of both entities (FLX predominantly positive and negative biochar surface). Since FLX exists predominantly in uncharged form, no electrostatic forces are expected at pH = 11.

Therefore, under typical electrostatic considerations, maximum adsorption of FLX is expected at pH 9, where FLX is positively charged while biochar carries a negative charge. However, the observed adsorption order (pH 11 > 9–5 > 6.5 > 3) deviates from the classical electrostatic expectations. In the present study, the maximum adsorption was observed for pH 11 (as shown in Fig. 4a), where FLX is predominantly neutral and electrostatic attraction is minimal. The findings suggest that there is no significant effect of on the adsorption of FLX on biochar (p value < 0.05) and electrostatic interactions are not the primary forces driving the adsorption. In addition, no appreciable changes (p value < 0.05) in the adsorption of FLX on biochar on varying the concentration of NaCl from 0.01 to 0.1 to 0.5 M (Fig. 4b) further strengthen that electrostatic forces play only a minor role. Further, the heteroatom-rich, negatively charged surface functional groups, such as –C–O–C–, C=O, –C–O–, –OH, –NH(R), can establish hydrogen bonding with the protonated amine (–NH$_2$) functionality of FLX.[42,43]

Besides electrostatic forces and hydrogen bonding, FLX can also base hydrophobic–hydrophobic (van der Waals interaction), attractive interactions, owing to the hydrophobic nature

of both-the biochar surface and the target pollutant.[40] The octanol partition coefficient of FLX (K_{ow} of 4.17) indicates the hydrophobic nature of the pharmaceutical compound and its tendency to adsorb on a solid surface rather than remain in the aqueous phase.[44,45] However, co-solvent experiments using methanol (2.5–10% v/v) revealed no appreciable changes in the adsorption (p value < 0.05), thereby suggesting hydrophobic interactions do not play a dominant mechanism either (as shown in Fig. 4c). If hydrophobic interactions were central, the presence of methanol would disrupt the hydrophobic partitioning of FLX into the biochar matrix, thereby affecting the adsorption process.

Moreover, low desorption using solvents, methanol, acidic methanol (pH 2), and 50% ACN, also suggests strong and irreversible adsorption, like pore entrapment, or strong coordination of FLX with the surface functional groups of biochar, rather than electrostatic and hydrophobic forces. The aromatic rings in the structure of FLX can serve as the π-electron acceptors for the carbon-based biochar, which can typically conform as robust π-donors due to the presence of oxygen-rich function groups, such as hydroxyl.[19,31,40,43] In addition, the microporosity of the olive-stone biochar, coupled with high surface area (855 m^2 g^{-1}), is also expected to greatly contribute to the adsorption of small organic polar molecule, FLX, on the biochar surface.[40] Thereby, for FLX, non-electrostatic and non-hydrophobic interactions, such as pore filling, hydrogen bonding or complexation with functional groups, and π–π EDA forces are expected to play a significant role in adsorption on olive-stone-derived CO$_2$- activated biochar.

4. Conclusions

In the present study, olive stone waste was used as a carbon precursor to produce biochar, which was employed to remove FLX from aqueous solutions. The study of adsorption kinetics demonstrated that the pseudo-second-order kinetic model best described the experimental data with a regression coefficient of >0.99. The process is also driven by intra-particle diffusion, with a direct correlation between initial FLX concentration and the intra-particle diffusion constant. Further, both Langmuir and Freundlich's isotherm models were in good agreement with the experimental data, with good regression coefficients. Model

parameters, including R_L (between 0.324 and 0.986, *i.e.*, $0 < R_L < 1$), and K_F (>1), suggested favourable irreversible adsorption of FLX onto the biochar for initial FLX concentrations varying from 1 to 50 mg L^{-1}. Further, the maximum adsorption capacities ranged from 4.82 ± 0.04 mg g^{-1} to 146.45 ± 10.55 mg g^{-1}, for initial FLX concentrations of 1 mg L^{-1} to 50 mg L^{-1}, respectively, which exceeds the adsorption capacity of previously reported waste-derived biochar used for FLX removal.

The findings also suggest a significant contribution of pore entrapment, hydrogen bonding, and π–π EDA forces in the adsorption of FLX on olive-stone-derived CO_2-modified biochar, and a minor contribution from the electrostatic attractive and hydrophobic–hydrophobic forces. Overall, the study shows that agri-food waste-derived biosorbents can be a potential alternative to produce high-capacity adsorbents for industrial applications while sustaining the vision of a circular economy and waste valorization.

Data availability

The data supporting this article have been included in the ESI.†

Author contributions

Pratishtha Khurana: conceptualization, visualization, investigation, writing original draft preparation, data curation and analysis; Samreen Sran: investigation, writing original draft preparation; Ratul Kumar Das: conceptualization, reviewing, editing; Luz Sanchez-Silva: reviewing; Satinder Kaur Brar: reviewing, supervision, funding acquisition.

Conflicts of interest

The authors declare that they have no known competing financial interests or persona; relationships that could have appeared to influence the work reported in this paper.

Acknowledgements

References

1 R. Brauer, B. Alfageh, J. E. Blais, E. W. Chan, C. S. L. Chui, J. F. Hayes, K. K. C. Man, W. C. Y. Lau, V. K. C. Yan, M. Y. Beykloo, Z. Wang, L. Wei and I. C. K. Wong, *Lancet Psychiatry*, 2021, **8**, 1071–1082.

2 M. L. García-García, C. A. Tovilla-Zárate, M. Villar-Soto, I. E. Juárez-Rojop, T. B. González-Castro, A. D. Genis-Mendoza, M. Á. Ramos-Méndez, M. L. López-Nárvaez, A. S. Saucedo-Osti, J. A. Ruiz-Quiñones and J. J. Martinez-Magaña, *Psychiatry Res.*, 2022, **307**, 114317.

3 B. Pinto, D. Correia, T. Conde, M. Faria, M. Oliveira, M. do R. Domingues and I. Domingues, *Chemosphere*, 2024, **357**, 142026.

4 M. Deodhar, S. B. A. Rihani, L. Darakjian, J. Turgeon and V. Michaud, *Pharmaceutics*, 2021, **13**, 148.

5 J. M. Orozco-Hernández, G. A. Elizalde-Velázquez, L. M. Gómez-Oliván, G. O. Santamaría-González, K. E. Rosales-Pérez, S. García-Medina, M. Galar-Martínez and N. S. Juan-Reyes, *Sci. Total Environ.*, 2023, **905**, 167391.

6 D. Correia, I. Domingues, M. Faria and M. Oliveira, *Sci. Total Environ.*, 2023, **857**, 159486.

7 E. K. Richmond, E. J. Rosi, A. J. Reisinger, B. R. Hanrahan, R. M. Thompson and M. R. Grace, *J. Freshwater Ecol.*, 2019, **34**, 513–531.

8 D. Correia, I. Domingues, M. Faria and M. Oliveira, *Appl. Sci.*, 2022, **12**, 2256.

9 H. Sari Erkan, D. Kaska, N. Kara and G. Onkal Engin, *Environ. Technol.*, 2024, 1–14.

10 O. P. Togunde, K. D. Oakes, M. R. Servos and J. Pawliszyn, *Environ. Sci. Technol.*, 2012, **46**, 5302–5309.

11 A. Salahinejad, A. Attaran, D. Meuthen, D. P. Chivers and S. Niyogi, *Sci. Total Environ.*, 2022, **807**, 150846.

12 C. Pan, M. Yang, H. Xu, B. Xu, L. Jiang and M. Wu, *Chemosphere*, 2018, **205**, 8–14.

13 N. O. de Farias, R. Oliveira, P. N. S. Moretti, J. M. e Pinto, A. C. Oliveira, V. L. Santos, P. S. Rocha, T. S. Andrade and C. K. Grisolia, *Comp. Biochem. Physiol., Part C:Toxicol. Pharmacol.*, 2020, **237**, 108836.

14 B. R. Eisenreich, S. Greene and A. Szalda-Petree, *Physiol. Behav.*, 2017, **173**, 258–262.

15 OECD, *Pharmaceutical Residues in Freshwater: Hazards and Policy Responses*, Organisation for Economic Co-operation and Development, Paris, 2019.

16 T. L. Palma and M. C. Costa, *Anaerobe*, 2021, **68**, 102356.

17 Y. F. Velázquez and P. M. Nacheva, *Environ. Sci. Pollut. Res.*, 2017, **24**, 6779–6793.

18 M. J. Fernandes, M. M. Moreira, P. Paíga, D. Dias, M. Bernardo, M. Carvalho, N. Lapa, I. Fonseca, S. Morais, S. Figueiredo and C. Delerue-Matos, *Bioresour. Technol.*, 2019, **292**, 121973.

19 A. Lago, B. Silva and T. Tavares, *Sustainable Mater. Technol.*, 2024, **39**, e00792.

20 B. Silva, M. Martins, M. Rosca, V. Rocha, A. Lago, I. C. Neves and T. Tavares, *Sep. Purif. Technol.*, 2020, **235**, 116139.

21 M. Puig-Gamero, A. Esteban-Arranz, L. Sanchez-Silva and P. Sánchez, *J. Environ. Chem. Eng.*, 2021, **9(4)**, 105374.

22 B. Sajjadi, W.-Y. Chen and N. O. Egiebor, *Rev. Chem. Eng.*, 2019, **35**, 735–776.

23 J. Mathew, G. Bhardwaj, R. Pulicharla, P. Rezai and S. K. Brar, *Sci. Total Environ.*, 2024, **951**, 175595.

24 J. Lehmann and S. Joseph, *Biochar for Environmental Management: Science and Technology*, Earthscan, London; Sterling, VA, 2009.

25 C. Piccirillo, I. S. Moreira, R. M. Novais, A. J. S. Fernandes, R. C. Pullar and P. M. L. Castro, *J. Environ. Chem. Eng.*, 2017, **5**, 4884–4894.

26 S. Escudero-Curiel, U. Penelas, M. Á. Sanromán and M. Pazos, *Chemosphere*, 2021, **268**, 129318.

27 S. Escudero-Curiel, M. Pazos and A. Sanromán, *Environ. Pollut.*, 2023, **330**, 121751.

28 H. H. Farghal, M. Nebsen and M. M. H. El-Sayed, *J. Polym. Environ.*, 2023, **31**, 5338–5354.

29 A. Camiré, J. Espinasse, B. Chabot and A. Lajeunesse, *Environ. Sci. Pollut. Res.*, 2020, **27**, 3560–3573.

30 S. Escudero-Curiel, M. Pazos and A. Sanromán, *J. Mol. Liq.*, 2022, **357**, 119079.

31 G. Jaria, V. Calisto, M. V. Gil, M. Otero and V. I. Esteves, *J. Colloid Interface Sci.*, 2015, **448**, 32–40.

32 G. R. N. Nkana, A. Lajeunesse, B. Chabot and P. Nguyen-Tri, *J. Environ. Chem. Eng.*, 2024, **12**, 112228.

33 B. Y. Z. Hiew, L. Y. Lee, X. J. Lee, S. Gan, S. Thangalazhy-Gopakumar, S. S. Lim, G.-T. Pan and T. C.-K. Yang, *J. Taiwan Inst. Chem. Eng.*, 2019, **98**, 150–162.

34 A. Puga, M. Pazos, E. Rosales and M. A. Sanromán, *Chemosphere*, 2021, **280**, 130778.

35 J. Narayanan, J. G. Hernández, I. I. Padilla-Martínez, P. Thangarasu, S. E. Santos Garay, C. B. Palacios Cabrera and A. J. Santiago Cuevas, *Ceram. Int.*, 2021, **47**, 20544–20561.

36 M. M. Nassar, *Water Sci. Technol.*, 1999, **40**, 133–139.

37 X. Guo and J. Wang, *J. Mol. Liq.*, 2019, **296**, 111850.

38 C. Moreno-castilla, F. Carrasco-marín, F. J. Maldonado-hódar and J. Rivera-utrilla, *Carbon*, 1998, **36**, 145–151.

39 Q. Chen, H. Liu, Z. Yang and D. Tan, *J. Mater. Cycles Waste Manage.*, 2017, **19**, 256–264.

40 Z. Jeirani, C. H. Niu and J. Soltan, *Rev. Chem. Eng.*, 2017, **33**, 491–522.

41 L. S. Maia, A. I. C. da Silva, E. S. Carneiro, F. M. Monticelli, F. R. Pinhati and D. R. Mulinari, *J. Polym. Environ.*, 2021, **29**, 1162–1175.

42 I. Brás, L. Teixeira Lemos, A. Alves and M. F. R. Pereira, *Manag. Environ. Qual.*, 2004, **15**, 491–501.

43 S. M. Mahgoub, D. Essam, Z. E. Eldin, S. A. A. Moaty, M. R. Shehata, A. Farghali, S. E. B. Abdalla, S. I. Othman, A. A. Allam, F. I. A. El-Ela and R. Mahmoud, *Sci. Rep.*, 2024, **14**, 3990.

44 A. Aghababaei, V. B. Borugadda, A. Dalai and C. H. Niu, *Chem. Eng. Res. Des.*, 2023, **189**, 138–155.

45 A. D. M. Silva, D. F. Fernandes, S. A. Figueiredo, O. M. Freitas and C. Delerue-Matos, *Int. J. Environ. Res. Public Health*, 2022, **19**, 6081.